Electron transport in quantum dot solids: Monte Carlo simulations of the effects of shell filling, Coulomb repulsions, and site disorder

R. E. Chandler,[1] A. J. Houtepen,[2] J. Nelson,[1] and D. Vanmaekelbergh[2]

[1]*Department of Physics, Imperial College London, Prince Consort Road, London SW7 2BW, United Kingdom*
[2]*Debye Institute, Utrecht University, Princetonplein 1, 3508 TA, Utrecht, The Netherlands*

A Monte Carlo model is developed for the hopping conductance in arrays of quantum dots (QDs). Hopping is simulated using a continuous time random walk algorithm, incorporating all possible transitions, and using a nonresonant electron-hopping rate based on broadening of the energy levels through quantum fluctuations. Arrays of identical QDs give rise to electronic conductance that depends strongly upon level filling. In the case of low charging energy, metal insulator transitions are observed at electron occupation levels, $\langle n \rangle$, that correspond to the complete filling of an S, P, or D shell. When the charging energy becomes comparable to the level broadening, additional minima in conductance appear at integer values of $\langle n \rangle$, as a result of electron-electron repulsion. Disorder in QD diameters leads to disorder in the energy levels, resulting in washing out of the structure in the dependence of conductance on $\langle n \rangle$ and a net reduction in conductance. Simulation results are shown to be consistent with experimental measurements of conductance in arrays of zinc oxide and cadmium selenide QDs that have different degrees of size disorder, and the degree of size disorder is quantified. Simulations of the temperature dependence of conductance show that both Coulombic charging and size disorder can lead to activated behavior and that size disorder leads to conductance that is sublinear on an Arrhenius plot.

I. INTRODUCTION

Semiconductor quantum dots (QDs) small enough that electronic wave functions are confined within the nanocrystal volume may be considered as "designer atoms" on account of the possibility of controlling electronic structure by controlling the QD size. Assemblies of QDs condensed into QD solids can, in an analogous way, be considered as artificial or designer solids and can be prepared nowadays from many different nanocrystals, including ZnO,[1] CdSe,[2–4] and PbSe.[5] Electronic conductance in such solids is a function of the electronic interaction between QDs in the assembly, i.e., of the separation, intervening medium (barrier material), mechanism of charge transfer, and of the degree of disorder (in both size and packing) in the assembly as well as of the degree of shell filling due to conduction band electrons. The range of these parameters offers the possibility to explore electronic conductance in different physical regimes and, interestingly, the transitions between such regimes.

In assemblies of ZnO semiconductor QDs, the electronic transfer integral between neighboring QDs, $h\Gamma$, is expected to be only a fraction of an meV at room temperature[6] and therefore charge transport occurs by incoherent hopping between neighboring QDs. Within this weak coupling regime, hopping conductance depends upon level filling, giving rise to "filling controlled" metal-insulator transitions (MITs) with additional structure (bandwidth controlled MITs of the Mott-Hubbard variety[7]) introduced when the charging energy is significant. Conductance-level filling behavior is further influenced by disorder in site energies and hopping distance. Thus, by control of a few parameters, the characteristics of different transport regimes can be probed. Such studies are of great relevance both to the fundamental physical understanding of charge transport in solids and to the nascent applica-

tions of QD solids in areas such as single-electron transistors in logic circuits, and optoelectrical devices such as solar cells[8] and electrochemically gated low-threshold lasers.[9]

The dependence of conductance on level filling in QD solids has been studied experimentally by several research groups using the simple and elegant electrochemical gating method,[10] whereby the electronic Fermi level is controlled through an applied electrochemical potential, whilst conduction is probed via a small (∼10 mV) bias applied between two metal electrodes. Such studies have shown that QD solids display a dependence of conductance on $\langle n \rangle$ that is compatible with the filling of electron shells. In ZnO QD solids, conductance within the S shell, i.e., for $\langle n \rangle < 2$, is distinct from that via the P levels, occurring for $\langle n \rangle > 2$, and reflects the expected degeneracy of those shells.[10] With solids of CdSe nanocrystals, higher conductance was again observed for P-type conduction than S shell conduction, and, moreover, a maximum in the S-shell conductance was found at $\langle n \rangle = 1$.[3] These effects are completely analogous to the filling-controlled MITs that have been studied in transition metal compounds in which the electron occupation of narrow d bands was varied by means of chemical doping.[7]

In order to interpret the experimental results that have been reported and to explore possible novel conductance regimes which have not yet been accessed experimentally, a theoretical framework for electron transport in QD solids is desired. In the strong coupling regime, relevant, e.g., for metal nanoparticles, the different transport regimes can be described via a band structure calculation using the Mott-Hubbard Hamiltonian in the tight binding approximation,[11] but such studies are restricted to small systems with small occupation numbers. Disordered systems can be described qualitatively using models such as Mott's variable range hopping (VRH) (Ref. 12) and that due to Efros and

Shlovskii.[13] In the weak-coupling regime explicit modeling of disordered systems is feasible, since each state is localized on a single QD. Monte Carlo (MC) methods are well suited to the study of such systems as they readily allow the degree of disorder in QD size and packing to be varied, as well as the charging energy, occupation level and other parameters. Until recently, MC methods had been used only in a trivial way, to simulate hopping conduction in systems with only one level per nanocrystal.[14] Recently van de Lagemaat[15] presented a first MC model for conduction in QD solids at room temperature. His simulations focused on the Einstein relation between mobility and diffusion constant, especially at critical points in filling controlled MITs. The simulations were based on a limited set of energy levels per quantum dot, which limits accuracy, and were restricted to room temperature.

In this paper, we present a Monte Carlo–based study of electron transport in a small three-dimensional QD array, embedded between planar boundaries with different quasi-Fermi levels, which represent the source and drain electrodes of an electrochemically gated device. Conduction proceeds by hopping between the orbitals on neighboring quantum dots, according to a resonant tunneling rate based on quantum fluctuations in the energy levels. A continuous-time random walk algorithm is used to handle the multiple particles and levels in the system and only single orbital occupancy is allowed. We monitor the linear conductance as a function of $\langle n \rangle$ in order to study the effects of shell filling and address the behavior both in the regime of the monodisperse and perfectly ordered QD solid and in the regime of size disordered (and consequently energetically disordered) arrays. In each limit we study the effects of Coulomb blockade on the transport characteristics by varying the on-site repulsion energy with respect to kT. We also study the temperature dependence of conduction in the different cases, and show how features resulting from size disorder and from Coulombic repulsion are manifest in the T dependence. Finally, we compare our results with experimental data for ZnO and CdSe QD solids and interpret the behavior in terms of the model. The results obtained here form a sound basis for interpretation of the experimental results that have been acquired to date. The variety of possible transport features that we predict will help to guide future experimental research.

II. FORMULATION OF THE MODEL

Model of electron conduction in a quantum dot lattice

The quantum-dot assembly is modeled as a small three-dimensional cubic lattice of dimensions X, Y, Z where each of the $M = X \times Y \times Z$ sites contains a QD of diameter D centered on that lattice point. We consider only QD solids with a fully occupied valence band and conduction orbitals of various occupation. In such a system conduction is due to the motion of electrons only. Each QD can accommodate up to N_{levels} electrons in a set of N_{levels} singly degenerate orbitals with electron addition energies $E_N(D)$, measured relative to the conduction band edge of the bulk crystal. We consider systems containing up to 34 orbitals (two S levels, six P levels, ten D levels, two S^* levels, and fourteen F levels). For ordered systems all QD diameters are identical; otherwise,

the diameters D are distributed on a Gaussian distribution of width σ_D, truncated such that none of the dots' energy levels exceed the vacuum level of E_{vac} with respect to the conduction band edge (for ZnO, $E_{\text{vac}} = 3$ eV).

The system is used to simulate electron conduction in a miniature electrochemically gated QD assembly as follows. All QDs in the first ($z = 1$) lattice plane, representing the electron injecting electrode, are assigned a quasi-Fermi energy of $\tilde{\mu}_e + eV_{\text{sd}}/2$, while all QDs in the final ($z = Z$) lattice plane are assigned a quasi-Fermi energy of $\tilde{\mu}_e - eV_{\text{sd}}/2$, where $\tilde{\mu}_e$ is the applied electrochemical potential (which is equal to the Fermi level of the system), e is the electronic charge, and V_{sd} the applied source-drain bias; V_{sd} is only a small perturbation of the electrochemical potential. $\tilde{\mu}_e$ is determined by the mean occupation number $\langle n \rangle$ of the QDs and is obtained by solving the following equation:

$$\langle n \rangle = \frac{1}{M} \sum_{m=1}^{M} \left(\sum_{i=1}^{N_{\text{levels}}} \frac{1}{e^{[E_i(D_m) - \tilde{\mu}_e]/kT} + 1} \right), \quad (1)$$

where $E_i(D_m)$ is the electron addition energy of the ith level of the mth QD, k is Boltzmann's constant, and T is temperature. The quasi-Fermi energies of the electrode planes thus specify both the applied source-drain bias V_{sd} and the mean QD occupation $\langle n \rangle$. To simulate conductance as a function of temperature, we choose to keep $\langle n \rangle$ constant and recalculate the value of $\tilde{\mu}_e$ at each temperature. This approach is appropriate for a system (such as that studied in the last section of this paper) where the electrolyte is frozen after charging by the gate bias.

For given values of V_{sd} and $\langle n \rangle$, the steady-state source-drain current density J_{sd} is obtained as follows. At the start of the simulation, the orbitals of all nonelectrode or "central" QDs are occupied at random, roughly according to their Fermi-Dirac occupation probabilities, to achieve a mean density of $\langle n \rangle$ electrons per QD. Each orbital of each QD in each of the electrode planes is assigned a fractional occupation according to the Fermi-Dirac occupation function $f(E, E_F) = (e^{(E-E_F)/kT} + 1)^{-1}$, given the orbital energy E and the quasi-Fermi energy E_F ($= \tilde{\mu}_e \pm eV_{\text{sd}}/2$) for that electrode, and maintains that fractional occupation throughout the simulation.

At the start of the random walk the transition frequencies, $\Gamma_{a \to b}$, are calculated, as defined below, for all possible electron transitions from initial level a to final level b. Transitions are allowed from any occupied or partially occupied orbital of a QD to any unoccupied or partially occupied orbital in each of the six nearest-neighbor QDs. Hops to further neighbors are not taken into account. A wait time t_a is calculated for the electron in each occupied or partially occupied level,

$$t_a = -\frac{\ln \gamma}{\displaystyle\sum_{i=1}^{N_{\text{trans}}} \Gamma_{a \to i}}, \quad 0 \le \gamma < 1, \quad (2)$$

where N_{trans} is the number of possible transitions for the electron in level a. Following the continuous-time random-walk model developed by Nelson and Chandler,[16–18] the electrons

are sorted into the order of their wait times and the electron with the shortest wait time t_1 is selected. For this electron, a relative probability is defined for each possible transition:

$$P_b = \gamma_b - \gamma_{b-1}, \qquad (3)$$

where

$$\gamma_b = \sum_{i=1}^{b} \Gamma_{1 \to i} \Big/ \sum_{i=1}^{N_{\text{trans}}} \Gamma_{1 \to i}, \quad b = 1, \dots, N_{\text{trans}}. \qquad (4)$$

A particular transition, B, is selected by generating a random number, γ, between 0 and 1 and determining B such that $\gamma_{B-1} \le \gamma \le \gamma_B$.

The transition to level b is then performed, imposing periodic boundary conditions in the x and y directions. Note that if the transition implies electron extraction from or injection into one of the electrode planes, only the occupation of QDs in the central (i.e., nonelectrode) planes is actually changed; the fractional populations in the $z=1$ and $z=Z$ planes are maintained. The simulation time is advanced by t_1 and this walk procedure is repeated. The source-drain current density J_{sd} is sampled at intervals of 10 times the nearest neighbor hopping time from a singly occupied to an empty QD, using

$$J_{\text{sd}} = \frac{e \times \text{net electron transitions from } z=2 \text{ to } z=3}{\text{time interval} \times \text{cross sectional area}}. \qquad (5)$$

The random walk is continued until J_{sd} reaches a steady state value to within a tolerance of 10% and this value, averaged over 50 time intervals, is recorded. The process is repeated many (10^3–10^6) times for different realizations of the lattice with the same V_{sd} and $\langle n \rangle$, and an average J_{sd} is obtained. We have found J_{sd} to vary linearly with V_{sd} in all cases studied, for $-10 \text{ mV} \le V_{\text{sd}} \le 10 \text{ mV}$. Therefore, we use the value of J_{sd} at $V_{\text{sd}} = 10$ mV as a standard measure of conductivity $G = Z \times J_{\text{sd}} / V_{\text{sd}}$. The whole procedure is then repeated for different values of $\langle n \rangle$, charging energy, size disorder, or temperature, to study these influences on G. In some cases the differential mobility μ_{diff}, $\mu_{\text{diff}} = (1/e) dG/d\langle n \rangle$ is calculated by fitting the $G(\langle n \rangle)$ curve to a set of piecewise continuous nth order polynomials and differentiating.

Calculation of the electron addition energies

The electron addition energies, $E_N(D)$, representing the energy of the Nth electron added to a QD of diameter D are calculated from the expression

$$E_N(D) = \varepsilon_N(D) + (2N-1)E_c(D), \qquad (6)$$

where $\varepsilon_N(D)$ is the kinetic confinement energy, i.e., the difference between the single electron energy in a nanocrystal and in a bulk crystal of the same material, and E_c is the Coulombic charging energy. For our studies we use values of $\varepsilon_N(D)$ that have been calculated using a tight binding approach[19] for the S, P, D, S^*, and F levels in approximately spherical ZnO nanoparticles. The parametric forms used for the $\varepsilon_N (D)$ are given in the supplementary material.[20] Al-
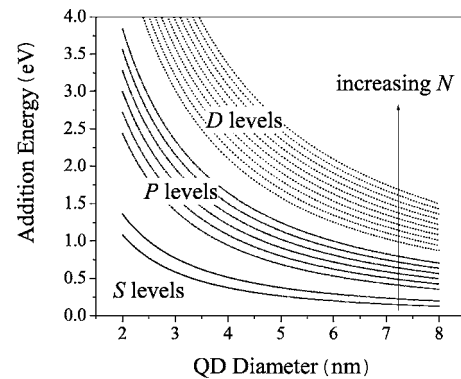

FIG. 1. The family of electron addition energy curves (S, P, and D levels) for $N=1$ up to $N=18$, and $A=0.28$ eV nm, calculated according to Eq. (6) using the formulas for the kinetic confinement energies of ZnO nanocrystals (Ref. 20).

though the values given there are specific to ZnO, the order and degeneracy of the levels is similar for all other wurtzite and zinc-blende quantum dots (such as CdSe, CdTe, and ZnSe). For semiconductor nanocrystals with a rocksalt structure (e.g., PbSe) the electronic structure is different; in that case the lowest energy level is eightfold degenerate.[21]

The second term in Eq. (6) represents the sum of two terms: The polarization energy and the electron-electron repulsion energy. Because the Coulomb interaction between two electrons is only weakly dependent on the angular momentum quantum number and because correlation effects between electrons are small (few meV) the polarization energy is well approximated by the Coulombic charging energy E_c upon addition of one electron to a QD of capacitance C, $E_c = e^2/2C$. If correlation effects between electrons are neglected, the repulsion energy due to the $N-1$ electrons already in the QD is given by $\sim 2(N-1)E_c$. This corresponds to the constant capacitance of electron addition, also known as the "standard model."[22] For a spherical QD E_c is inversely proportional to the QD diameter, hence

$$E_c = A_c/D, \qquad (7)$$

where A_c is a parameter incorporating the effect of the dielectric environment, which is inversely related to the relative permittivity of the QD material and the polarity of the surrounding electrolyte. The value of A_c is smaller for more polar experimental systems where Coulombic interactions are more easily screened. Figure 1 shows the electron addition energies as a function of D for the S, P, and D levels of a ZnO QD calculated using the formulas for $\varepsilon_N(D)$ given in the supplementary material[20] and $A_c = 0.28$ eV nm.[23]

To simulate size disorder, a Gaussian distribution in QD diameter is applied to the QDs in the assembly. We parametrize the resulting energetic disorder λ as the half-width at half maximum of the (slightly asymmetric) distribution in the lowest confinement energy (E_{S1}) that results from the Gaussian distribution in diameters. For example, a Gaussian distribution with $\sigma_D = 1$ nm around a mean D of 4.5 nm leads to $\lambda = 0.087$ eV.

Calculation of transition rates

For resonant tunneling between a level a in system A with density of states (i.e., degeneracy) g_a and a level b in system B with density of states g_b, the electron transfer rate $\Gamma_{a\rightarrow b}$ is given by

$$\Gamma_{a\rightarrow b}(E,E_F) = g_a(E)f(E,E_F)g_b(E)[1-f(E,E_F)]\beta_{ab}(E),$$

(8)

where β_{ab} is the resonant tunneling rate through the intervening (barrier) medium. Equation (8) expresses that the tunneling rate from a to b depends on both the concentration of electrons in the initial level and the concentration of vacancies in the final level. Under equilibrium conditions, the transition rate from a to b is equal to the transition rate from b to a, as required by detailed balance.

If the initial energy level E_a and final level E_b are not resonant, phonons have to be absorbed or emitted during the transition from a to b, in order to conserve energy. In analogy with the Marcus model for electron transfer[24] we assume here that the absorption or emission of a single phonon occasionally brings nonresonant levels into resonance at energy E. Electron-phonon interactions lead to a Gaussian broadening of the energy levels such that the probability of the level a being found at energy E is given by[25]

$$p_a(E) = \frac{1}{T\sqrt{2\pi k C_v}} \exp\frac{-(E-E_a)^2}{2kT^2C_v},$$

(9)

where E_a is the unbroadened energy level and C_v is the average single-phonon heat capacity of the nanocrystal material. C_v can be calculated for the semiconductor nanocrystals using the Debye model for the density of phonon states (see Ref. [20]). $p_a(E)$ may be considered as the time-averaged density of states associated with level a. A similar expression applies for the probability of the level b being found at E. For typical values of parameters for ZnO nanocrystals, the level broadening represented by Eq. (9) is several tens of meV at room temperature.

The transition rate from a to b in the nonresonant system is then obtained by substituting the effective density of states functions, $p_a(E)$ and $p_b(E)$ for g_a and g_b in Eq. (8) and integrating over energy:

$$\Gamma_{a\rightarrow b}(E_F) = \int_{-\infty}^{\infty} p_a(E)f_A(E,E_F)p_b(E)$$
$$\times [1-f_B(E_b,E_F)]\beta_{ab}(E)dE.$$

(10a)

The above integral cannot be solved analytically, but it is well approximated by the following expression:

$$\Gamma_{a\rightarrow b}(E_F) = f_A(E_a,E_F)[1-f_B(E_b,E_F)]$$
$$\times \frac{1}{\sqrt{8\pi k T^2 C_v}} \exp\left(-\frac{(E_a-E_b)^2}{4kT^2C_v}\right)$$
$$\times \beta_{ab}\exp\left(\frac{E_a-E_b}{2kT}\right).$$

(10b)

The Boltzmann factor in the rate $\Gamma_{a\rightarrow b}(E_F)$ results from the requirement that the system obeys detailed balance at equilibrium, as is usual with nonresonant electron transfer in fermionic systems.

The expression in Eq. (10a) was evaluated numerically for a range of parameters representative of the systems studied here, and it was confirmed to agree with the approximation in Eq. (10b) to within a few percent. The shape of the function described by Eq. (10b) is very similar to the line shape of the conductance through a single quantum dot obtained by Beenakker.[26]

According to the Wentzel-Kramers-Brillouin (WKB) approximation, the resonant tunneling rate β_{ab} is given by

$$\beta_{AB} = v_0 \exp\left[-\left(\frac{2m^*\left(E_{\text{vac}} - \frac{1}{2}(E_a+E_b)\right)}{\hbar^2}\right)^{1/2}\Delta x_{\text{edge}}\right],$$

(11)

where v_0 is a constant with the units of frequency, m^* is the electron effective mass, and Δx_{edge} is the shortest edge-to-edge distance between the original and final QD. It is assumed that β_{ab} is weakly dependent on the resonant transition energy, and the mean of E_a and E_b is taken as a representative value. The dependence on level energies of the transition rate $\Gamma_{a\rightarrow b}$ is mathematically analogous to the expression for small polaron hopping from Marcus theory,[24] with a reorganization energy of $C_v T$.

In the simulation, when calculating the transition rates using Eqs. (10b) and (11), we determine the fractional occupation factors f for all levels of QDs in the electrode planes using the quasi-Fermi level E_F for that electrode. For a level in a central (nonelectrode) QD, f is set equal to 1 or 0 depending on whether that level is occupied or not at that instant.

Tests of the model

The very large number of possible transitions even with a small assembly of QDs restricts the size of assembly that can be simulated in practice. Therefore, we have carried out preliminary tests in order to study the sensitivity of results to the system size and to the number of levels included. In Fig. 2(a) the simulated differential mobility, i.e., $\mu_{\text{diff}}(\langle n\rangle) \sim dG/d\langle n\rangle$, is shown as a function of occupation level for assemblies of $2\times2\times3$ identical QDs, including S, P, D, and S^* levels, and $3\times3\times4$ identical QDs, including S, P, D, S^*, and F levels. Small differences in the conductivity will be enhanced in the differential mobility, which therefore serves as a sensitive probe. The figure shows that $\mu_{\text{diff}}(\langle n\rangle)$ is virtually independent of system size and of number of levels included for the systems studied. As size disorder is increased small deviations in $\mu_{\text{diff}}(\langle n\rangle)$ appear at high $\langle n\rangle$. Figure 2(b) shows simulated conductivity as a function of $\langle n\rangle$ for a size-disordered system incorporating different numbers of orbitals. This shows that all of the S, P, D, S^*, and F levels must be included to calculate conductivity correctly for size-disordered systems with occupation numbers greater than seven. Simulations including such large numbers of levels are very costly to run and required the use of a distributed processing grid. Therefore, we have dealt with smaller occu-
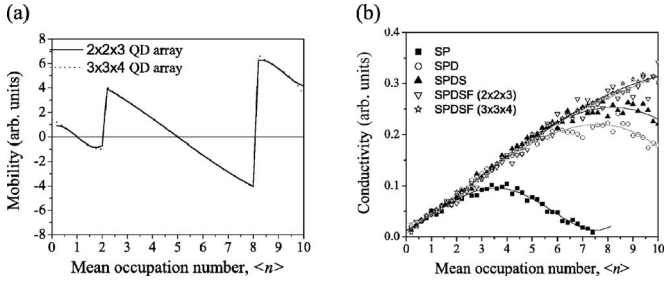
(a)

(b)

FIG. 2. (a) Differential mobilities calculated from fourth order polynomial fits to the simulated conductivity $G(\langle n \rangle)$ data for an array of $2 \times 2 \times 3$ identical QDs with $SPDS^*$ levels and a $3 \times 3 \times 4$ identical QD array with $SPDS^*F$ levels. The QD diameter is $D=4.5$ nm, and charging energy $Ec=2.2$ meV ($A_c=0.01$ eV nm). (b) Conductivity as a function of $\langle n \rangle$ for a size disordered system with $2 \times 2 \times 3$ QDs and $\sigma_D=1$ nm [$\lambda=87$ meV] as a function of the number of levels included. Increasing numbers of levels are needed to calculate G correctly at high $\langle n \rangle$. The two curves for S, P, D, S^*, and F are for assemblies of $2 \times 2 \times 3$ (open triangles) and $3 \times 3 \times 4$ (open stars) QDs, showing excellent agreement. Full lines are to guide the eye. The QD diameter is $D=4.5$ nm and $E_c=2.2$ meV.

pation numbers, and therefore smaller total numbers of levels, wherever possible. Figure 2(b) again shows agreement between conductivity using assemblies of $2 \times 2 \times 3$ and $3 \times 3 \times 4$ QDs, in the case of the S, P, D, S^*, and F levels. The two comparisons give confidence in the use of small systems to simulate the bulk properties of the QD assembly, and also emphasize that large numbers of levels are needed to properly simulate size disordered systems with large $\langle n \rangle$. We emphasize that although the systems are small, the fact that we studied very many realizations (10^3–10^6) of the system allows us to investigate the effects of size disorder (see below).

III. RESULTS AND DISCUSSION

Effects of shell filling and charging energy on the transport characteristics in ideal QD solids

First we consider the effects of level filling and charging energy in the case of an ideal assembly of quantum dots without any size dispersion and no packing disorder. Figure 3(a) shows the conductivity at room temperature as a function of $\langle n \rangle$ for a system of identical 4.5 nm QDs for low ($E_c=2.2$ meV) and high ($E_c=62$ meV) values of the charging energy. In the case of a very small charging energy [upper plot in Fig. 3(a)] three regimes are visible: A regime between 0 and 2 electrons per quantum dot, corresponding to the S conduction orbitals, a regime between 2 and 8 electrons per quantum dots (P orbitals), and a regime of 8 or more electrons per quantum dot (D orbitals). Within the shown range of $\langle n \rangle$, there are two metal-insulator transitions (MITs), where the conductivity is strongly decreased. The system becomes insulating when, for every level in the system, either the initial state is empty or the final state is full. At $\langle n \rangle=2$, all S orbitals are full and all P orbitals are empty, apart from the small overlap between the S and P levels due to phonon broadening, and so conductivity is very small.
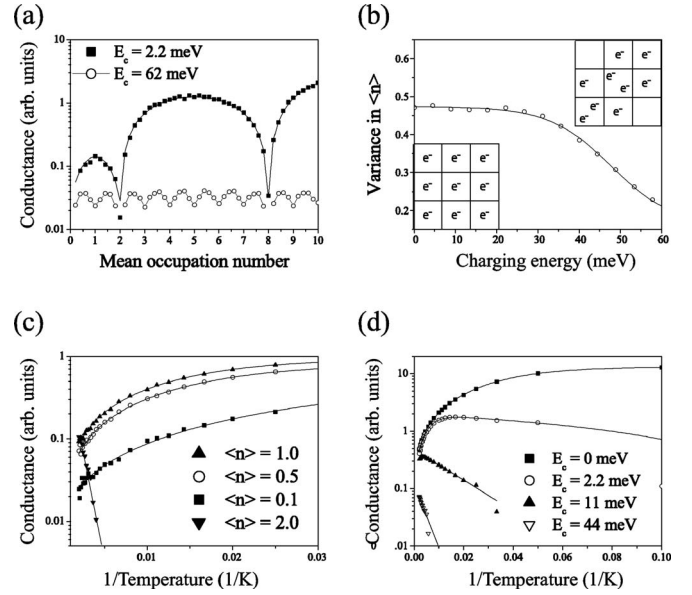
(a)

(b)

(c)

(d)

FIG. 3. (a) Room-temperature conductivity as a function of the mean occupation number $\langle n \rangle$ for an array of ideal $2 \times 2 \times 3$ identical QDs of 4.5 nm diameter, for charging energies of $E_c=2.2$ meV (filled squares) and $E_c=62$ meV (open circles). (b) The variance in the electron occupation of a QD in the central plane of the array as a function of charging energy, showing that a high charging energy leads to ordering of electrons in the array. The insets show schematic snapshots of the electron distribution: The left lower snapshot corresponds to large charging energy and low variance; the right upper snapshot corresponds to small charging energy and high variance. (c) Arrhenius plot of conductivity for the system in part (a) with $E_c=2.2$ meV, at different electron occupation levels: $\langle n \rangle=0.1$ (squares), 0.5 (circles), 1.0 (upward triangles), and 2.0 (downward triangles). (d) Arrhenius plots of conductivity for the system in part (a) at $\langle n \rangle=3$ with different charging energies, $E_c=0$ (filled squares), 2.2 meV (open circles), 11 meV (upward triangles), and 44 meV (downward triangles). In all plots, full lines are to guide the eye.

This overlap, and the resulting conductivity, reduce further with decreasing temperature. For values of $\langle n \rangle$ not corresponding to filled shells, electron transfer is generally possible between all the orbitals in the unfilled shell provided that the charging energy E_c separating the orbitals is small compared to kT. This is the case for $E_c=2.2$ meV in Fig. 3(a). Note that the conductivity is maximized in the S regime for $\langle n \rangle=1$ and in the P regime for $\langle n \rangle = 5$. For a system with degenerate orbitals in each shell, these points correspond to the cases when $f=0.5$.

A very different behavior is observed when the charging energy is larger than kT [lower plot in Fig. 3(a), $E_c=62$ meV]. Here conductivity reaches a minimum at every integer value of $\langle n \rangle$, leading to ten MITs over the range of $\langle n \rangle$ shown. Likewise, G is maximized at every half integer value of $\langle n \rangle$. Now, because $E_c > kT$, the energy separation between orbitals within a given shell has become significant, i.e., the degeneracy of the shells is lifted. Every time an orbital is completely filled (integer $\langle n \rangle$), the resonant transitions are shut off, and the conductivity is minimal. For example, at $\langle n \rangle=1$, at low kT, there is exactly one electron in every QD in the array. Then transitions within the first S
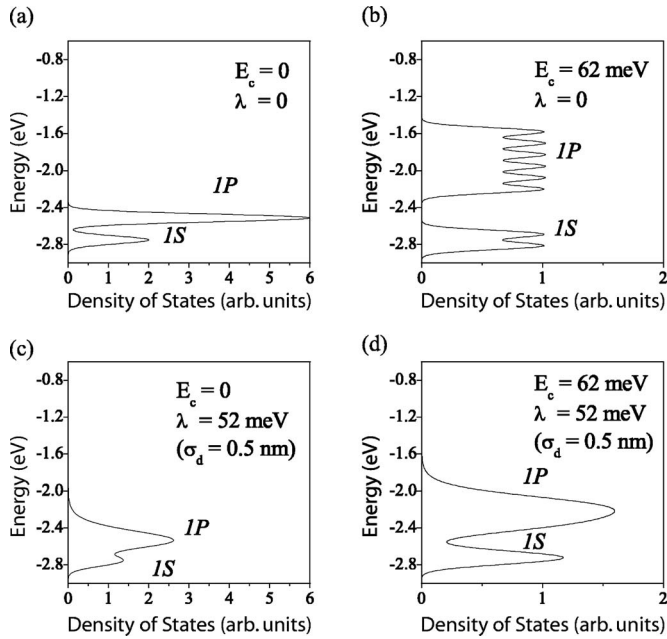
FIG. 4. Calculated density of states functions for the S and P levels of an assembly of ZnO QDs of mean diameter 4.5 nm, at room temperature. (a),(b) No size disorder and (a) $E_c=0$ and (b) $E_c=62$ meV. (c),(d) same as (a), (b) with a standard deviation of 0.5 nm in QD diameter, corresponding to a size disorder parameter of 52 meV.

level, S_1, are closed because $(1-f)=0$; transitions within S_2 and higher levels are closed because $f=0$, and the only possible transitions, which involve adding a second electron to an occupied QD, require an energy input of E_c. This type of MIT, which results from the charging energy, is known as a *Mott-Hubbard MIT*. Similar Mott-Hubbard type MITs were observed in simulations by van de Lagemaat.[15]

In order to illustrate the influence of the underlying density of states (DOS) on conductance, we have calculated the distributions of S and P level energies in a system of ZnO QDs of mean diameter 4.5 nm, for different values of E_c. For each of the S and P levels, the mean level energy was calculated using Eq. (6) and a Gaussian broadening applied to each level using Eq. (9). This thermal broadening, of 42 meV is the same for all levels at room temperature. Figure 4(a) shows that, for a system of identical QDs with E_c $=0$, the density of states is strongly peaked at the S and P energies, but drops towards zero at an energy intermediate between the S and P bands. The low DOS at this intermediate energy explains why nonresonant tunneling between S and P levels is highly unlikely, and as a result the conductance is minimized at $\langle n \rangle=2$, as shown in the conductance plots in Fig. 3(a). Figure 4(b) illustrates the case of identical QDs when $E_c=62$ meV. The effect of the charging energy in separating out the S and P levels is evident. The minima in the DOS in between each level are responsible for the minima in the conductance at integer $\langle n \rangle$, shown in Fig. 3(a) for $E_c=62$ meV. Figures 4(c) and 4(d) illustrate the effect of size disorder on the density of states in each case. Strong size disorder washes out the minima in the DOS, resulting in higher probability of transitions between different bands, as we shall see below.

The effect of increasing charging energy on the electron distribution in a QD solid is demonstrated in Fig. 3(b). This figure shows the variance in electron occupation for a QD in the central plane of a dot in a $2 \times 2 \times 3$ array as a function of E_c when $\langle n \rangle=1$. For low E_c the variance is large, corresponding to frequent changes in the electron occupation. For large E_c, the variance is small; multiple occupation of any QD corresponds to a large energy cost. It is clear that, for a QD solid with no size disorder, the effect of a large E_c is to tend to equalize the orbital occupation [lower left inset panel in Fig. 3(b)]. This charge ordering is similar to that in a Wigner crystal.

Interestingly, the maximum values of the conductivity can be related to the relevant degeneracy of states in the low E_c and high E_c limit. For $E_c \gg kT$, only the highest unfilled orbital contributes to conduction at any $\langle n \rangle$, so the maximum transition rate occurs when $\langle n \rangle - \text{int}(\langle n \rangle)=0.5$ ($f=0.5$) and is proportional to 0.25β [see Eq. (8)], since the degeneracies of the initial and final state are one. For $E_c \ll kT$, all the orbitals in the unfilled (twofold degenerate) shell contribute to conduction. Therefore the maximum conductance in the S shell is expected to occur when $\langle n \rangle=1$ ($f=0.5$) and to be proportional to 1.0β. Similarly the maximum conductance for the P shell when $E_c \ll kT$ is expected to be proportional to 9β.

The simulation results in Fig. 3(a) show clearly that, when $E_c \ll kT$, the ratio between the maximum of the S shell conductivity and the maximum of the P shell conductivity is 1:9, while the maximum of conductivity in the high E_c (Mott Hubbard) case is one-quarter of that for the S shell conductivity in the low E_c case. This suggests that the relative magnitude of conductivity at different $\langle n \rangle$ is a good indicator of the degeneracy of levels taking part in the conduction.

We now address the temperature dependence of the conductance. As described above, the transition rates depend upon the heat capacity C_v which is, in general, temperature dependent. In order to more clearly distinguish the effects of level filling, charging energy, and size dispersion on conductance we use a temperature independent (room-temperature) C_v for the present. In the last section of this paper we will incorporate the temperature dependence of C_v.

The presence of MITs leads to strong variations in the temperature dependence of the conductance. This is illustrated in Fig. 3(c), which shows the Arrhenius plot of G for an ideal array of $2 \times 2 \times 3$ identical QDs when E_c $=2.2$ meV (filling controlled regime). At an orbital occupation that corresponds to a critical point in an MIT, the conductivity increases with increasing temperature: At $\langle n \rangle=2.0$ the conductivity exhibits almost perfect Arrhenius behavior (the difference will be discussed below), with an activation energy of ~ 110 meV. In this situation conduction is only possible by adding an electron to a P orbital, thus by overcoming an energy barrier that is similar to the S-P separation. In such a situation, the expected activation energy is equal to the difference between the first P orbital energy and the Fermi level. Taking into account only the first S and first P levels, and given that the S-P energy gap is much larger than kT, the Fermi energy is given by

$$E_F = \frac{E_S + E_P}{2} + \frac{kT}{2} \ln \frac{g_S}{g_P}, \qquad (12)$$

where g_S (g_P) is the degeneracy of the S (P) shell. Using the energy levels for ZnO at $D=4.5$ nm, this leads to a Fermi energy of 133 meV below the first P level at 300 K, in good agreement with the observed activation energy.

At $\langle n \rangle$ values not corresponding to filled shells, conductivity depends weakly on T and actually *decreases* with increasing temperature over the range 25 to 300 K. This inverse temperature behavior is a consequence largely of our choice to conserve $\langle n \rangle$ rather than E_F as T is varied. As T is increased, with $\langle n \rangle$ conserved, transitions against the electron concentration gradient introduced by the applied bias become relatively more likely. Thus thermal diffusion increasingly washes out the small bias used for these simulations. If E_F were conserved rather than $\langle n \rangle$, thermally activated conductivity would result because the increased population of all levels above E_F and the increased vacancies in levels below E_F, both tend to increase the $f(1-f)$ product in Eq. (8). It should be noted that electron-phonon scattering, which could alternatively explain the negative T dependence of conduction, is not incorporated in our simulations.

Figure 3(d) shows conductivity curves at $\langle n \rangle = 3$ for different values of the charging energy. It is clear that as E_c is increased, conductivity becomes more strongly activated, with an activation energy that is similar to E_c. For example, the activation energy of the simulation with $E_c = 44$ meV is 21 meV, which is in excellent agreement with the expected value of $(1/2)$ E_c, given that the Fermi level should lie midway between the two S levels when $\langle n \rangle = 1$ [Eq. (12)]. Such behavior has been observed experimentally, where charging energy was varied through choice of electrolyte in an electrochemically gated system.[6] The data in Fig. 3(d) clearly indicate that Coulombic charging alone can cause activated conduction. At high T the inverse T behavior becomes more prominent, clearly indicating competition between two mechanisms, with the activated behavior due to Coulombic charging becoming more prominent as the Mott-Hubbard gap develops. Activated behavior due to charging is also seen in the data in Fig. 3(c) when taken to lower temperature (10–20 K). In this regime G increases with increasing temperature for $\langle n \rangle = 0.5$ and $\langle n \rangle = 1.0$, with an activation energy of ~2 meV. Using Eq. (12) with equal degeneracy for the different levels, the Fermi energy at $\langle n \rangle = 1$ is midway between S orbitals and the expected activation energy is $(1/2)$ E_c, which corresponds to 1.1 meV, in reasonable agreement with the simulated value.

In general, three domains can be identified in the temperature dependent conductivity of arrays of identical QDs: An activated domain (insulator) where a shell is completely occupied, resonant transitions are blocked, and the energy difference between different shells has to be overcome; an activated domain (insulator) where an orbital within an unfilled shell is filled, resonant transitions are blocked, and the charging energy has to be overcome by the thermal energy; and a nonactivated domain (metallic conductor) where resonant transitions are always allowed.
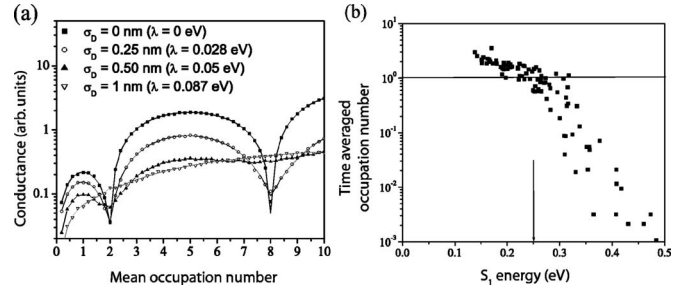

FIG. 5. (a) Conductivity as a function of the mean occupation number at 300 K for an array of $3 \times 3 \times 4$ QDs with $E_c = 2.2$ meV and different size-disorder parameters: No disorder ($\lambda=0$ meV, filled squares), weak disorder ($\lambda=28$ meV, open circles), medium disorder ($\lambda=56$ meV, filled upward triangles), and strong disorder ($\lambda=87$ meV, open downward triangles). The filling controlled MITs become increasingly washed out as the size disorder increases. (b) The average QD occupation as a function of the $S1$ energy level for QDs in the central plane of a $3 \times 3 \times 4$ array with $E_c = 2.2$ meV and $\lambda=87$ meV. The vertical arrow shows the value of E_{S1} for a QD with $D=4.5$ nm. Small QDs, with a higher E_{S1}, quickly become unpopulated and do not participate in conduction.

Effects of size dispersion on the transport characteristics

To investigate the effects of size disorder, we carried out conductance simulations on arrays of QDs whose diameters are drawn from a Gaussian distribution of width σ_D. As described above, we use the half-width at half maximum, λ, of the resulting distribution in $1S$ energies as a parameter for the size disorder. Figure 5(a) shows simulated conductance as a function of $\langle n \rangle$ for four different values of λ for a $3 \times 3 \times 4$ array of QDs with $E_c = 2.2$ meV. To allow for wide variations in site energy the full set of energy levels, S, P, D, S^*, and F were included. As shown in the figure, the effect of increasing size disorder is to decrease the magnitude of the conductivity and to wash out the minima in conductance at the critical (filling controlled) occupation levels. The reduced conductance at mid-shell $\langle n \rangle$ values results from the difference in energy levels of neighboring QDs such that tunneling is in general nonresonant and never reaches the ideal rate given by Eq. (8). The loss of the clear MIT features is due to the overlap of the distributions of S and P shells, such that no value of $\langle n \rangle$ exists which results in completely filled shells. This is evident from the density of states functions of the size disordered system shown in Figs. 4(c) and 4(d), where it is clear that there is no energy in the S-P regime where the transition rate vanishes at room temperature, irrespective of the value of E_c. We find that for a size disorder of $\lambda \sim 2kT$ the MITs are still visible, whereas above this size disorder all features of the transitions are gone. If the charging energy is sufficiently low ($E_c \ll kT$) the conductance versus $\langle n \rangle$ plots can give an idea of the degree of energy level disorder in the solid.

One additional reason for the decrease in conduction observed in Fig. 5(a) is illustrated in Fig. 5(b). Here, the time-averaged occupation of a QD in the central plane of an array with $\langle n \rangle = 1$ is shown as a scatter plot against the lowest S orbital energy, E_{S1}, of the QD. Small QDs, i.e., those which have E_{S1} larger than the E_{S1} that corresponds to the mean QD
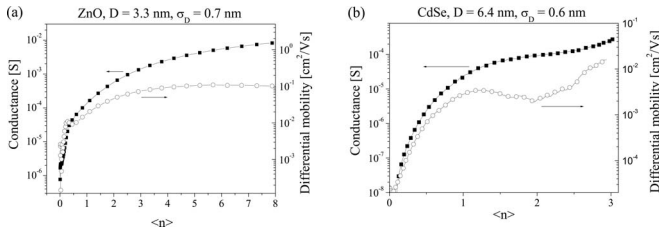
FIG. 6. Room temperature conductance and differential mobility in arrays of (a) ZnO nanocrystals of mean diameter 3.3 nm and large size dispersion of ~0.7 nm ($>20\%$) and (b) CdSe nanocrystals of mean diameter 6.4 nm and small size dispersion of ~0.6 nm ($<10\%$).

diameter (marked by the arrow), have a much lower occupation than the mean value of 1. Since such nanocrystals are hardly ever populated by an electron, they form "hostile" sites in the conduction path, similar to impurity scatterers in a metal or semiconductor, and tend to decrease the average current through the array. A final reason for the lower conductivity in the disordered system is the "trapping" of electrons in lower lying levels of large dots. The net effect of size disorder is thus to decrease the transition rate and to increase the spread of rates (tending to cause dispersive transport) and also to distort the conduction pathways through the system.

The washing out of filling controlled MITs can also be seen experimentally in ZnO QD arrays at room temperature (see also Ref. 10). Figure 6(a) shows the conductance (filled squares) and differential mobility (open circles) of an array of 3.3 nm ZnO nanocrystals as a function of the mean electron occupation $\langle n \rangle$. (Experimental details are given as supplementary material.[20]) The experimentally observed conductance strongly resembles the simulated curve with $\lambda = 87$ meV which corresponds to a size dispersion of 22%. The size dispersion of the experimental ZnO particles is estimated to be 20%.[27] In systems with a smaller size dispersion some features of the MIT are retained. This is the case for arrays of CdSe particles as shown in Fig. 6(b) (see also Ref. 3) and has also been shown for arrays of PbSe nanocrystals.[5] In Fig. 6(b) the conductance is shown for an array of 6.4 nm CdSe nanocrystals with a size dispersion of ~10%. A shoulder is visible in the conductance and a clear minimum is observed in the differential mobility at $\langle n \rangle \approx 2$, corresponding to a fully occupied S shell. The experimental conductance resembles the simulated curve with $\lambda = 56$ meV in Fig. 5(a), corresponding to a size dispersion of ~11%, although some caution should be taken in comparing experimental results for CdSe QDs with simulations that are based on ZnO nanocrystals.

Disorder in site energies is expected to lead to activated conduction, because the transition rate for nonresonant tunneling increases with increasing thermal fluctuations. The temperature dependence of conductivity is shown in Fig. 7(a) for a size-disordered $2 \times 2 \times 3$ QD array with $E_c = 2.2$ meV and $\lambda = 87$ meV, at $\langle n \rangle = 1$ (black squares). Weakly activated behavior is shown with an activation energy of around 10 meV. This value may be influenced by both disorder and Coulombic charging. Therefore, also shown on Fig. 7(a) are the temperature dependent conductance data for this system
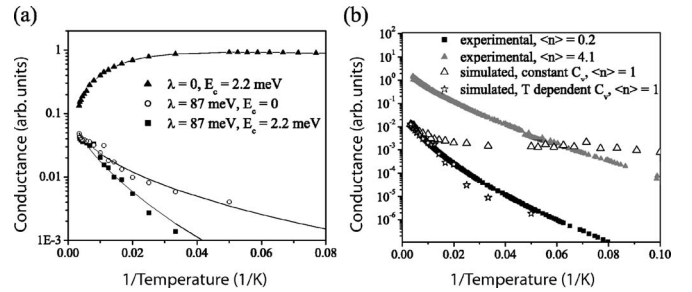

FIG. 7. (a) Arrhenius plot of conductivity for a system of 4.5 nm ZnO quantum dots at $\langle n \rangle = 1$ with both size disorder and charging energy (squares), with size dispersion only (circles) and with charging energy only (triangles). (b) Experimental conductance data for an electrochemically gated 3.3 nm QD array at two different values of the mean occupation level, $\langle n \rangle = 0.2$ (filled squares) and $\langle n \rangle = 4.1$ (filled triangles), compared with simulated conductance for an array of 3.3 nm QDs with $E_c = 60$ meV and size disorder $\lambda = 50$ meV, with temperature independent C_v for $\langle n \rangle = 1$ (open triangles). The result for $\langle n \rangle = 1$ when a T dependent C_v is used is also shown (open diamonds). Solid lines are guides to the eye.

with Coulombic charging alone, and with size disorder alone. Although the small E_c is insufficient to lead to activated behavior in the temperature range shown, it does appear to *enhance* the activation energy of the size-disordered system. Simulations of size-disordered systems with larger values of E_c show qualitatively similar behavior with weak, sublinear T dependence on an Arrhenius plot. The case of $E_c = 60$ meV and $\lambda = 50$ meV, at $\langle n \rangle = 1$ is shown in Fig. 7(b) (open triangles). The strong effect of E_c on activation energy that is observed for ordered systems with filled levels [Fig. 3(d)] is thus lost in size-disordered systems, where the energy step for conductance in a filled-level system is no longer well defined. From these studies it is clear that the influences of E_c and size disorder are complex and cannot, in general, be resolved from the experimental T dependence of conduction alone.

The sublinear behavior of the Arrhenius plots of conductance can be understood as follows: The effective activation energy E_a is determined by pathways that are responsible for the largest fraction of the current. At low temperature the conductance is dominated by the pathway with the lowest activation energies. As the temperature increases, the low activation-energy pathways become T independent ($kT \gg E_a$) and other pathways become important as well. This means that the average activation energy *increases*.

An additional factor which can influence the T dependence of conductivity is the T dependence of the nanocrystal heat capacity, C_v [see Eq. (10b)]. Until this point, the calculation of the level broadening was carried out using the value of C_v at 300 K, in order to more clearly distinguish the effects of charging and size disorder. To take into account the temperature dependence of C_v, we use the Debye model (see Ref. 20), according to which C_v should vary with T^3. In Fig. 7(b) the simulated T dependent conductivity of a $2 \times 2 \times 3$ array of 3.3 nm ZnO nanocrystals obtained using this T dependent form for C_v is shown (open diamonds) in comparison with the case of constant C_v (open triangles). It is clear that the activation energy is much larger than for the constant C_v case.

We now compare our simulations with the T dependent conductivity of an experimental QD array. In Fig. 7(b), the experimental temperature dependence of the conductance of an electrochemically gated array of 3.3 nm ZnO nanocrystals at two different electron concentrations are shown (experimental details can be found in the supplementary material[20]). The behavior is clearly sublinear on an Arrhenius scale, with a low-temperature activation energy of <10 meV. The trend is the same for the two different electron concentrations shown, and the activation energy decreases with increasing $\langle n \rangle$. The simulated curves in Fig. 7(b), obtained for parameters appropriate for this experimental system ($D=3.3$ nm, $E_c=60$ meV and $\lambda=50$ meV) and $\langle n \rangle=1$ exhibit qualitatively similar behavior to the experimental ones with a sublinear Arrhenius temperature dependence. [The T dependence of the simulated conductance for different $\langle n \rangle$ (not shown) is similar.] However, the magnitude of the slope of the Arrhenius plot is only reproduced in the case when C_v is temperature dependent. This shows that the T dependence of C_v cannot be ignored for a quantitative interpretation of experimental results.

Although the sublinear behavior can be explained by a competition of pathways through the system with different activation energies, this is not the only possible explanation. The temperature dependent conductance of arrays of other types of nanocrystals has previously been attributed to variable range hopping (VRH) in the Coulomb-gap regime, leading to a $\ln G \sim T^{-0.5}$ dependence[28] or to a combination of VRH and "activated behavior"[29] leading to a dependence of $\ln G \sim T^{-a}$, with $0.5 < a < 1.0$. Our work shows that such T dependence of conductance may also be attributed to the effect of particle-size disorder within the weak coupling regime. Further experimental work on systems with controlled disorder is needed to clarify whether the T dependence of conductivity is sufficient to distinguish between variable-range hopping and nearest-neighbor hopping mechanisms.

CONCLUSIONS

We have shown that the electronic conductance of an array of semiconductor quantum dots is a complex function of the QD dimensions, electrostatic environment (i.e., charging energy), and the degree of disorder. Monte Carlo simulations of electron hopping, using a nonresonant tunneling rate based on thermally induced level broadening, predict distinct regimes of conductance behavior: Metal-insulator transitions for ordered systems with filled shells, with additional MITs

for filled levels if the electron-electron repulsion is sufficiently high, while size disorder washes out these transitions and reduces overall conductance. The model is capable of distinguishing the conductance behavior in experimental systems that are known to possess a different degree of size disorder and producing a reasonable quantitative estimate of that disorder. The comparison shows that reduced dispersion in QD size is a clear objective, in order to obtain higher conductance and sharper dependence of conductance on level filling, a feature that could be exploited in devices. The microscopic model is costly to run because of the large number of levels that must be included in size disordered systems and has thus far been restricted to very small arrays. Extension to more realistic systems that also include features such as packing disorder would require the development of approximate descriptions of the electron transfer rates between multiple level, multiply occupied QDs.

The temperature dependence of conduction is key in determining the nature of charge transport at a microscopic level. In this paper we have shown that the exact T dependence of conduction in a QD solid is the result of several cooperative or competing factors: Thermal activation due to charging, thermal activation due to site energy disorder, and inverse temperature behavior due to diffusion when $\langle n \rangle$ is conserved with T. The latter phenomenon may play a role in electrochemically gated QD solids in which a constant concentration of electrons are "frozen." In addition to these factors are the temperature dependence of the heat capacity, which is not yet fully understood for nanoparticles, and the nature of conductance in conditions where μ_e should be conserved rather than $\langle n \rangle$, which will also lead to strongly activated behavior. It is clearly difficult to assign hopping mechanisms on the basis of the T dependence of conductance alone without additional studies, such as the dependence of G on $\langle n \rangle$, to ascertain the relative importance of E_c and size disorder. These considerations will become particularly important when attempting to compare different transport theories in the analysis of the low T behavior of systems that approach the coherent hopping regime.[29]

[1] A. L. Roest *et al.*, Faraday Discuss. **125**, 55 (2004).

[2] C. B. Murray, C. R. Kagan, and M. G. Bawendi, Annu. Rev. Mater. Sci. **30**, 545 (2000).

[3] D. Yu, C. J. Wang, and P. Guyot-Sionnest, Science **300**, 1277 (2003).

[4] A. J. Houtepen and D. Vanmaekelbergh, J. Phys. Chem. B **109**, 19634 (2005).

[5] B. L. Wehrenberg *et al.*, J. Phys. Chem. B **109**, 20192 (2005).

[6] A. L. Roest, J. J. Kelly, and D. Vanmaekelbergh, Appl. Phys. Lett. **83**, 5530 (2003).

[7] N. F. Mott, *Metal-Insulator Transitions* (Taylor & Francis, London, 1990).

[8] R. J. Ellingson *et al.*, Nano Lett. **5**, 865 (2005).

[9] C. J. Wang *et al.*, J. Phys. Chem. B **108**, 9027 (2004).

[10] A. L. Roest, J. J. Kelly, D. Vanmaekelbergh, and E. A. Meulenkamp, Phys. Rev. Lett. **89**, 036801 (2002).

[11] F. Remacle and R. D. Levine, ChemPhysChem **2**, 20 (2001).

[12] N. F. Mott, *Conduction in Non-Crystalline Materials* (Clarendon Press, Oxford, 1993).

[13] A. L. Efros and B. I. Shklovskii, J. Phys. C **8**, L49 (1975).

[14] E. Lampin, C. Delerue, M. Lannoo, and G. Allan, Phys. Rev. B **58**, 12044 (1998).

[15] J. van de Lagemaat, Phys. Rev. B **72**, 235319 (2005).

[16] A. N. M. Green *et al.*, J. Phys. Chem. B **109**, 142 (2005).

[17] J. Nelson, Phys. Rev. B **59**, 15374 (1999).

[18] J. Nelson and R. E. Chandler, Coord. Chem. Rev. **248**, 1181 (2004).

[19] Y. M. Niquet, Ph.D. thesis, University des Sciences et Technologies Lille, 2001.

[20] See EPAPS Document No. E-PRBMDO-75-029708 for formulas used for calculation of kinetic confinement energies in ZnO nanocrystals, for a derivation of the Debye heat capacity for nanocrystals, and for details on the experimental data presented. For more information on EPAPS, see http://www.aip.org/pubservs/epaps.html.

[21] P. Liljeroth, P. A. Zeijlmans van Emmichoven, S. G. Hickey, H. Weller, B. Grandidier, G. Allan, and D. Vanmaekelbergh, Phys. Rev. Lett. **95**, 086801 (2005).

[22] D. V. Averin, A. N. Korotkov, and K. K. Likharev, Phys. Rev. B **44**, 6199 (1991).

[23] A. L. Roest, Ph.D. thesis, Dept. of Chemistry, University of Utrecht, Utrecht, 2003.

[24] R. A. Marcus, Angew. Chem., Int. Ed. Engl. **32**, 1111 (1993).

[25] F. Mandl, *Statistical Physics* (John Wiley and Sons, New York, 1988), p. 57.

[26] C. W. J. Beenakker, Phys. Rev. B **44**, 1646 (1991).

[27] E. A. Meulenkamp, J. Phys. Chem. B **102**, 5566 (1998).

[28] D. Yu, C. Wang, B. L. Wehrenberg, and P. Guyot-Sionnest, Phys. Rev. Lett. **92**, 216802 (2004).

[29] F. Remacle *et al.*, J. Phys. Chem. B **107**, 13892 (2003).